J. Opt. A: Pure Appl. Opt. **2** (2000) 216–222. Printed in the UK PII: S1464-4258(00)08670-0

Polarimetry using liquid-crystal variable retarders: theory and calibration

Juan M Bueno

Universidad de Murcia, Laboratorio de Óptica, Campus de Espinardo (Edificio C), 30071 Murcia, Spain

E-mail: bueno@fcu.um.es

Received 13 October 1999, in final form 21 January 2000

Abstract. A Mueller-matrix polarimeter in transmission mode using two electronically controlled liquid-crystal variable retarders has been developed. Its design, theory and calibration are described. Although liquid crystals have been proposed earlier, this paper is focused on the process of the calculation of the Mueller matrix by a matrix-inversion method, oriented to static systems and *in vitro* samples. By driving the retarders with appropriate voltages, nine independent pairs of polarization states can be produced (incomplete polarimetry), while the other additional seven pairs are obtained by placing two quarter-wave plates (in the input and output optical paths respectively). This configuration allows extraction of 16 independent measurements of intensity. The Mueller matrix of the sample is calculated from them. The results of Mueller matrices for air, a linear polarizer and a quarter-wave plate are presented. Additional polarization parameters such as retardation, ellipticity or degree of polarization were also computed and some applications of the system are proposed.

Keywords: Polarimetry, liquid crystal, Mueller matrix

1. Introduction

Mueller-matrix polarimeters (or ellipsometers) have been widely used to measure different polarization properties in optical systems and samples [1–5]. Most of these systems were based on fixed linear polarizers and rotating retarders, both in the generator and analyser paths. They normally used a Fourier analysis of the detected signal to obtain the Mueller matrix of the media under study [6, 7]. Hauge [8] reviewed the limitations of that kind of polarimeter and studied the information that could be obtained. Some systems only used rotating polarizers [9], but as they did not contain compensating elements, the complete Mueller matrix could not be obtained.

More efficient polarimetric systems have used electro-optical modulators [10, 11], Pockels cells [12, 13] or photoelastic modulators [14–18] instead of rotatory elements. Azzam [19] developed a faster polarimeter, based on a division-of-amplitude technique, in order to obtain the four parameters of each Stokes vector simultaneously. This system has recently been implemented [20–24].

Liquid-crystal (LC) devices are optically anisotropic media that act locally as a uniaxial retardation plate and exhibit optical birefringence [25]. They produce different polarization states depending on the external applied voltage and therefore can also be used in polarimeters [26–28]. These voltage-controlled LC devices are being used in many different applications ranging from optical rotators [29,30] or protection sensors [31], to wavefront corrector devices [32,33].

Recently a Mueller-matrix imaging polarimeter [34] using LCs adapted to an ophthalmoscopic double-pass apparatus [35] has been proposed, in order to calculate spatially resolved Mueller matrices of the human eye. In this work the theoretical basis of that system is described: a polarimeter using a pair of LC variable retarders (LCVR), both in the input and output optical paths. As is well known the first LCVR acts as a polarization-state generator (PSG) and the second as a polarization-state analyser (PSA). For a fixed position generator–analyser, only nine elements of the Mueller matrix can be obtained; the other seven will be accessible when two quarter-wave retarders (one behind the PSG and other in front of the PSA) are introduced. In this way, 16 intensities are recorded, each corresponding to a different independent combination of states PSG–PSA. With this set of intensities the Mueller matrix of the sample and its polarization properties can be computed.

In section 2, a description of the experimental set-up is presented. Details of the theory of the polarimeter are given in section 3. The calibration of the LCVRs is described in section 4. Some results are shown in section 5; a summary and some conclusions are presented in section 6.

2. Experimental set-up: polarimeter in transmission mode

Figure 1 shows a schematic diagram of the LCVR polarimeter. The light source is a 633 nm He–Ne laser.

1464-4258/00/030216+07$30.00

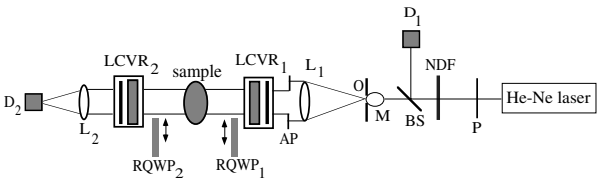

Figure 1. Schematic diagram of the LCVR polarimeter in transmission mode. P, polarizer; NDF, neutral density filter; BS, pellicle beam splitter; D_1 and D_2, linear photodetectors; M, microscope objective; O, pinhole; L_1 and L_2, lenses; AP, aperture; $LCVR_1$ and $LCVR_2$, liquid-crystal variable retarders; $RQWP_1$ and $RQWP_2$, removable quarter-wave plates.

Light passes through a polarizer (P) and a neutral density filter (NDF). Part of the light is reflected in a pellicle beam splitter (BS) and reaches a linear photodetector (D_1) used to measure reference intensities and correct the mean final intensity, according to fluctuations of the source. The laser beam is expanded by a microscope objective (M) and filtered by a pinhole (O). A lens L_1 ($f_1' = 100$ mm) collimates the beam, the size of which is controlled by the aperture AP. The first $LCVR_1$ (linear polarizer followed by a LC cell) acts as the PSG. A removable quarter-wave plate ($RQWP_1$) produces the fourth independent polarization state, as will be shown in section 3. After passing through the sample, the light enters the PSA. In the analyser path, another removable quarter-wave plate ($RQWP_2$) is placed in front of the second $LCVR_2$ (LC cell followed by a linear polarizer). A lens L_2 ($f_2' = 100$ mm) focuses the beam on a second linear photodetector (D_2). A PC controls the LCVRs and data recorded by photodetectors.

3. Theory

Each LCVR consists of an horizontal linear polarizer (OX-axis) in conjunction with a LC. The Stokes vector of the light going into the first LC is $(I_p, I_p, 0, 0)^T$. The Mueller matrix of a LC with retardation δ, and azimuthal angle of the fast axis α, is given by [36]:

$$M_\delta^\alpha = \begin{pmatrix} 1 & 0 & 0 & 0 \\ 0 & c^2 + s^2\cos\delta & sc(1-\cos\delta) & -s\sin\delta \\ 0 & sc(1-\cos\delta) & s^2 + c^2\cos\delta & c\sin\delta \\ 0 & s\sin\delta & -c\sin\delta & \cos\delta \end{pmatrix} \tag{1}$$

where $c = \cos 2\alpha$ and $s = \sin 2\alpha$. Due to a fixed angle between the principal axis of the linear polarizer and the fast axis of the LC (horizontal and 45° apart, respectively), the Stokes vector generated by the PSG is

$$S_{\mathrm{PSG}} = \begin{pmatrix} S_0 \\ S_1 \\ S_2 \\ S_3 \end{pmatrix} = I_p \begin{pmatrix} 1 \\ \cos\delta(V) \\ 0 \\ \sin\delta(V) \end{pmatrix} \tag{2}$$

where $\delta(V)$ is the retardation as a function of the applied voltage. Since S_2 is zero for any voltage, the azimuth of the ellipse of polarization [37] is always horizontal and all polarization states S_{PSG} are placed along a single meridian of the Poincaré sphere [38]. This means that, by driving the LCVRs, only changes in the ellipticity of the generated states are produced, as figure 2 shows.

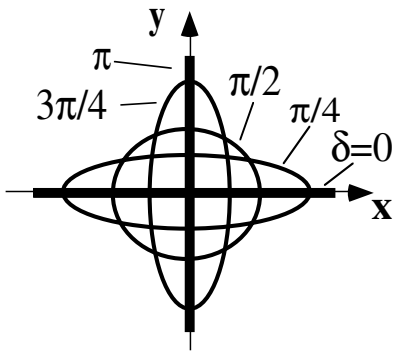

Figure 2. Ellipses of polarization corresponding to states S_{PSG}, as a function of the voltage applied to the LC.

The Mueller matrix of the system M, transforms the input Stokes vector S_{PSG} into the output Stokes vector S'. This system changes the polarization state of the light and possibly partially depolarizes it. In the PSA, the azimuthal angle of the fast axis of the LC is $-45°$ and the polarizer is also horizontal. The resulting Mueller matrix of the PSA is

$$\begin{aligned} \overline{M}_{\mathrm{PSA}} &= M^0_{\mathrm{pol}} \cdot M^{-45}_{\delta'} \\ &= \tfrac{1}{2}\begin{pmatrix} 1 & \cos\delta'(V') & 0 & \sin\delta'(V') \\ 1 & \cos\delta'(V') & 0 & \sin\delta'(V') \\ 0 & 0 & 0 & 0 \\ 0 & 0 & 0 & 0 \end{pmatrix} \end{aligned} \tag{3}$$

where V' is the external voltage applied to the second LC and δ', the retardation corresponding to this voltage. In summary, every Stokes vector S_{PSG} through the entire set-up becomes S_{D}, given by the simple matrix equation

$$S_{\mathrm{D}} = \overline{M}_{\mathrm{PSA}} \cdot M \cdot S_{\mathrm{PSG}} \tag{4}$$

where the first element of S_{D} is the intensity of the light reaching the photodetector [39] that can be written as:

$$\begin{aligned} I_{\mathrm{D}} = \frac{I_p}{2}&[m_{00} + m_{01}\cos\delta(V) + m_{03}\sin\delta(V)] \\ &+ [m_{10} + m_{11}\cos\delta(V) + m_{13}\sin\delta(V)]\cos\delta'(V') \\ &+ [m_{30} + m_{31}\cos\delta(V) + m_{33}\sin\delta(V)]\sin\delta'(V'). \end{aligned} \tag{5}$$

This expression of the intensity does not depend on the time, but includes nine terms depending on the retardations of LCVRs and the elements of the Mueller matrix of the sample. This implies that at one time only nine elements (neither the third row nor the third column) of the Mueller matrix can be computed. Therefore, as every recorded intensity implies the combination of nine elements, at least nine independent equations are required to calculate those elements. A method to infer the rest of the elements of the Mueller matrix M will be described in the following.

To obtain the 16 elements of the Mueller matrix, four independent polarization states in each unit (both PSG and PSA) are needed. In mathematical terms, four 4×1 vectors are independent if the determinant of the 4×4 matrix composed by them is not (or even close to) zero. For Stokes vectors, the largest possible value of this determinant is 2 (total independence) and in that case, three vectors are perpendicular to each other in the Poincaré sphere and the fourth is orthogonal (opposite direction) to one of them.

Because of the location of all S_{PSG} in a single plane, only three independent states of polarization can be produced (as the PSA is similar due to its symmetrical arrangement). The method used to obtain the fourth independent is based on the use of two removable quarter-wave plates, one in the PSG and other in the PSA. The effect of a quarter-wave plate is to rotate the incident Stokes vector at an angle of 90° around its fast axis in the counter-clockwise. The optimum azimuthal angle of the plate was calculated and a value of zero was obtained.

When inserting the $\lambda/4$ behind $LCVR_1$, the Stokes vector $S_{PSG}^{(\lambda/4)}$ emerging from it will be

$$S_{PSG}^{(\lambda/4)} = M_{\lambda/4}^{0} \cdot S_{PSG} = t_1 \cdot \begin{pmatrix} 1 & 0 & 0 & 0 \\ 0 & 1 & 0 & 0 \\ 0 & 0 & 0 & 1 \\ 0 & 0 & -1 & 0 \end{pmatrix} \cdot S_{PSG}$$

$$= t_1 \cdot I_p \begin{pmatrix} 1 \\ \cos\delta(V) \\ \sin\delta(V) \\ 0 \end{pmatrix} \tag{6}$$

where $M_{\lambda/4}^{0}$ is the Mueller matrix of the plate and t_1 its transmittance (previously measured).

If t_2 is the transmittance for the second $\lambda/4$, the Mueller matrix for the PSA when inserting the plate in front of $LCVR_2$ will be given by

$$\overline{M}_{PSA}^{(\lambda/4)} = M_{pol}^{0} \cdot M_{\delta'}^{-45} \cdot M_{\lambda/4}^{0}$$

$$= \frac{t_2}{2} \begin{pmatrix} 1 & \cos\delta' & -\sin\delta' & 0 \\ 1 & \cos\delta' & -\sin\delta' & 0 \\ 0 & 0 & 0 & 0 \\ 0 & 0 & 0 & 0 \end{pmatrix}. \tag{7}$$

Let M_{PSG} and M_{PSA} be the auxiliary 4×4 matrices for both the PSG and the PSA:

$$M_{PSG} = \begin{pmatrix} 1 & 1 & 1 & 1 \\ \cos\delta_1 & \cos\delta_2 & \cos\delta_3 & \cos\delta_4 \\ 0 & 0 & 0 & \sin\delta_4 \\ \sin\delta_1 & \sin\delta_2 & \sin\delta_3 & 0 \end{pmatrix}$$

$$M_{PSA} = \begin{pmatrix} 1 & \cos\delta_1' & 0 & \sin\delta_1' \\ 1 & \cos\delta_2' & 0 & \sin\delta_2' \\ 1 & \cos\delta_3' & 0 & \sin\delta_3' \\ 1 & \cos\delta_4' & -\sin\delta_4' & 0 \end{pmatrix} \tag{8}$$

where M_{PSG} is the matrix in which columns are the four independent Stokes vectors S_{PSG} (equations (2) and (6)), and M_{PSA} is the matrix with each row being the first row of every $\overline{M}_{PSA}$ (equations (3) and (7)). Although transmittances of plates (t_1 and t_2) have been omitted in expression (8) in order to understand the process more easily, they were always included when experimental measurements were carried out.

In this way, retardations δ_i and $\delta_i'(i = 1, 2, 3, 4)$ of the LCs associated to the largest values of the determinants of auxiliary matrices of equation (8) must be calculated. Since, after calibrating each LCVR (see section 4), both minimum and maximum retardations are known, the eight required retardations are computed. These values of retardation for $\delta_1, \delta_2, \delta_3, \delta_1', \delta_2'$ and δ_3' produce polarization states that are linear vertical (state 2), right circular (state 3) and approximately linear horizontal (state 1). In addition, $\delta_4 = \delta_3$ and $\delta_4' = \delta_3'$ were obtained.

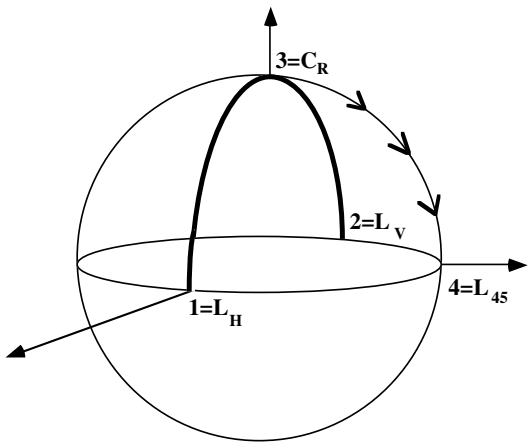

Figure 3. Location on the Poincaré sphere of the four independent polarization states. The effect of the quarter-wave plate is shown by arrows. The numbers associated to every polarization state are: state 1, linear horizontal (L_H); state 2, linear vertical (L_V); state 3, right circular (C_R) and state 4, 45° linear (L_{45}).

Table 1. Values of determinants (absolute value) used by different authors. The first one corresponds to our experimental setup. Determinants of series 2, 3, 4 and 5 correspond to references 40, 41, 42 and 43, respectively. The largest possible value of the determinant is 2.

Series	det
1	1.8
2	0.5
3	1
4	1.4
5	2

In view of these results, placing the quarter-wave plate (fast axis in horizontal position) behind the PSG, when right circular light is emerging ($\delta_3 = \pi/2$) 45° linear light (state 4) will be produced. The combination of this state 4 (in both generator and analyser units) with states 1, 2 and 3 will allow us to obtain the seven left PSG–PSA combinations to calculate the rest of the elements of the Mueller matrix. Figure 3 shows the location on the Poincaré sphere of the four independent Stokes vectors.

In table 1 the absolute value of the determinant for this work compared with that of others from the bibliography are shown. The second row is the determinant resulting from a rotatory polarimeter with equiangular increments of 22.5° given by Morgan *et al* [40]. The third determinant was used by Pezzaniti and Chipman [41], Ambirajan and Look [42] obtained the fourth value and Pelz *et al* [13] used the fifth. The present determinant is lower than 2 because the state 1 does not correspond exactly to linear horizontal light due to some properties of the LC cell (section 4). However, through this work, state 1 will usually be called L_H (assignment corresponding to a linear horizontal state (see figure 3)).

The calculation of the complete Mueller matrix involves 16 independent equations of intensity measurements. With the four independent states in every LCVR, 16 independent PSG–PSA combinations termed by i–j $(i, j = 1, 2, 3, 4)$ are produced. Nine elements of the Mueller matrix can be calculated at any one time and the rest result from the use of the removable quarter-wave plates. There are 16 intensities

distributed in four 4×1 flux-vectors $I_D(i)$ $(i = 1, 2, 3, 4)$ where a flux-vector corresponds to a fixed PSG state and four PSA states. The relationship between every Stokes vector $S'^{(i)}$ going out of the sample and the final intensities is given by (t_2 has not been included):

$$I_D(i) = \begin{pmatrix} I_d^{(1-1)} \\ I_d^{(1-2)} \\ I_d^{(1-3)} \\ I_d^{(1-4)} \end{pmatrix} = \tfrac{1}{2} \cdot M_{PSA} \cdot S'^{(i)}$$

$$= \tfrac{1}{2} \begin{pmatrix} 1 & \cos\delta'_1 & 0 & \sin\delta'_1 \\ 1 & \cos\delta'_2 & 0 & \sin\delta'_2 \\ 1 & \cos\delta'_3 & 0 & \sin\delta'_3 \\ 1 & \cos\delta'_4 & -\sin\delta'_4 & 0 \end{pmatrix} \begin{pmatrix} S_0'^{(i)} \\ S_1'^{(i)} \\ S_2'^{(i)} \\ S_3'^{(i)} \end{pmatrix}. \quad (9)$$

The inversion of the last equation for every $I_D(i)$ yields the four unknown Stokes vectors $S'^{(i)}$. If $M_{S_{OUT}}$ is the auxiliary 4×4 matrix with its columns being the four Stokes vectors $S'^{(i)}$ ($M_{S_{OUT}} = [S'^{(1)} S'^{(2)} S'^{(3)} S'^{(4)}]$), the experimental Mueller matrix of the sample can be obtained as a result of

$$M = M_{S_{OUT}} \cdot (M_{PSG})^{-1} \quad (10)$$

where M_{PSG} is the auxiliary matrix of equation (8).

4. Calibration of the LCVRs

To measure accurately the elements of the Mueller matrix, an independent calibration for every LCVR must be performed. For this we need to know the relation between the voltage applied to the LC and the retardation produced.

Once the two LCVRs were aligned in the straight-through configuration, the calibration was made placing the LC between crossed linear polarizers. Since a horizontal linear polarizer is placed inside every LCVR, only one external vertical polarizer is required (behind the PSG for $LCVR_1$ and in front of the PSA for $LCVR_2$).

If I_p is the intensity of the light entering the LC, the intensity reaching the detector when placing between crossed linear polarizers is:

$$I_{crossed} = I_p \sin^2\left(\frac{\delta}{2}\right) \quad (11)$$

where δ is the retardation of the LC for each value of voltage. Since I_p is known and $I_{crossed}$ is measured, for every applied voltage the retardation can be calculated as:

$$\delta = 2 \cdot a\sin\left(\sqrt{\frac{I_{crossed}}{I_p}}\right). \quad (12)$$

In figure 4 the retardation of a LCVR is plotted versus the external applied voltage. The input voltage is 0–5 V and the basic cell of LC does not reach a zero retardation state due to surface pinning effects from the alignment layer. Even at high voltages a residual retardation is present. One typical polarization state for the minimum retardation has been $S_{PSG}(\delta_{min}) = (1, 0.98, 0, 0.19)^T$. At low voltages large retardations can be obtained with small changes in the input signal, although a large inertia is also present.

The time of response of these devices depends on several parameters, including thickness of the LC layer, viscosity, temperature, nature of the drive voltage and the LC alignment geometry. Times ranging from 0.75 to 0.90 ms were found for the LCs used in the present work.

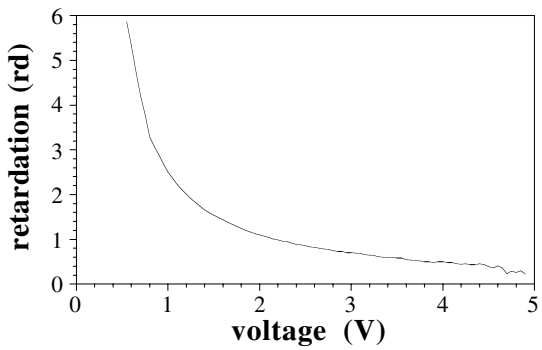

Figure 4. Calibration data for one of the LCVRs.

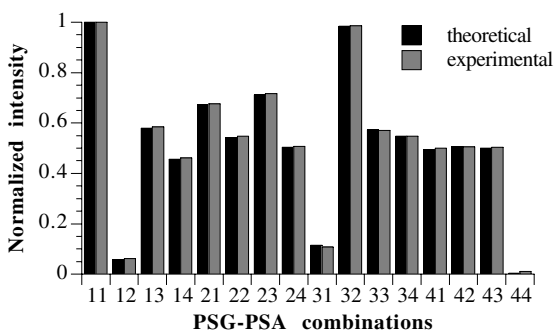

Figure 5. Theoretical and experimental intensities for each PSG–PSA combination, with the air as a test sample in the polarimeter.

For a fixed wavelength, the transmittance of the LC is uniform across the aperture and does not depend on the voltage. In this case, variations were lower than 0.1%.

5. Results

In order to verify the reliability of the polarimeter, three examples for test measurements of well-defined optical-polarization components are shown in this section. These experimental Mueller matrices provide the precision of the set-up and the accuracy of the results.

5.1. Example 1: the air

The 4×4 identity matrix is the Mueller matrix of the air. An example of experimental values obtained for this Mueller matrix has been:

$$M_{AIR} = \begin{pmatrix} 1 & 0.006 & 0.006 & 0.001 \\ -0.007 & 1.003 & 0.014 & 0.006 \\ 0.002 & -0.001 & 0.991 & 0.005 \\ -0.002 & 0.002 & 0.001 & 0.999 \end{pmatrix}.$$

The comparison of this result with the ideal matrix, shows a method to test the quality of the experimental system. Systematic errors are similar to other results in the literature [4,10–12]. Figure 5 shows the comparison between theoretical and experimental intensities recorded for the air.

Table 2. Parameters of polarization corresponding to experimental Mueller matrices of a quarter-wave-plate with its fast axis at -45°, 0°, 30° and 90°, 0° and 90° expected for ellipticity and retardation respectively.

	-45°	0°	30°	90°
Retardation	91.96 ± 0.70	91.74 ± 1.20	90.53 ± 1.42	92.67 ± 0.20
Azimuth	-44.29 ± 0.17	0.24 ± 0.11	30.74 ± 0.23	87.89 ± 0.63
Ellipticity	-2.05 ± 1.11	0.86 ± 0.44	3.59 ± 1.10	0.36 ± 0.07

5.2. Example 2: horizontal linear polarizer

The normalized Mueller matrix obtained for a linear polarizer with its transmission axis in horizontal position was

$$M_p^{0^\circ} = \begin{pmatrix} 1 & 1.013 & 0.018 & -0.014 \\ 1.027 & 1.041 & 0.010 & 0.009 \\ 0.024 & 0.040 & 0.020 & 0.014 \\ -0.021 & -0.019 & 0.016 & -0.024 \end{pmatrix}.$$

5.3. Example 3: a quarter-wave plate

In this last example the Mueller matrix for a quarter-wave plate is presented. The azimuth of the fast axis of the retarder was horizontal:

$$M_{\lambda/4}^{0} = \begin{pmatrix} 1 & 0.003 & 0.001 & 0.000 \\ 0.001 & 0.999 & 0.041 & 0.021 \\ -0.012 & -0.019 & -0.042 & 0.999 \\ 0.003 & 0.044 & -0.998 & -0.041 \end{pmatrix}.$$

If it is supposed that the elements of the first column and first row are not null because of small effects of depolarization, the polar decomposition for non-depolarizing optical systems [43] can be used to obtain the parameters of polarization (92.41° for retardation, 0.33° for azimuth and 0.86° for ellipticity were obtained). The value of ellipticity indicates that the retarder is linear. The degree of polarization [44] and the two principal coefficients of transmission [43] are close to 1. The coefficients of transmission show that the quarter-wave plate is a total retarder without diattenuation [45].

Errors in elements of the Mueller matrices may be due to slight misalignments of the different optical components, imperfections and internal reflections in test samples or small errors in the calibration of the LCVRs.

On the other hand, in table 2 values of parameters of polarization for different angles of the fast axis of the plate are shown. Each value is the average of three measurements and errors represent the standard deviation.

6. Discussion and summary

The experimental set-up and operation of a polarimeter consisting of a pair of LCVRs have been described. With this configuration and driving properly the LCVRs, only nine elements of the Mueller matrix of the sample can be obtained. In this way, since the Stokes vectors are not completely measured, incomplete polarimetry [1, 2] is involved. This technique can be used when the complete Mueller matrix is not needed, for instance, in the analysis of highly linear birefringent samples with minuscule amounts of other forms of polarization. In those cases, the system is usually known as a polariscope. Some polariscopes using rotatory elements and LCVRs have been recently proposed [46, 47].

However, a complete determination of the elements of the Mueller matrix using LCVRs requires the use of two additional removable quarter-wave plates. The intensities recorded for each PSG–PSA combination only depend on the retardation of the LCVRs and the elements of the Mueller matrix of the sample. This Mueller matrix is obtained by means of an easy matrix inversion method and a Fourier analysis of the signal is not required.

As examples, results of experimental Mueller matrices for the air, a linear polarizer and a quarter-wave plate have been shown. From the accuracy of these optical elements and the consideration of alignment errors, the error inherent is estimated at 2–4%, depending on the Mueller-matrix element.

Although it is well known that there are faster systems than the present one (see the introduction to this paper), the polarimetry using LCs has been successfully applied to measure polarization properties of the human eye using double-pass retinal images [35, 48].

Using LCVRs, errors caused by moving parts unavoidable when using mechanical rotation (inertia with its acceleration and brake times, misalignments of the signal on the detector, etc), are eliminated. Precise rotation stages, stepper motors and accessories such as a gearbox are dispensable. To produce a large retardation, very high voltages are not required. Different wavelengths can be used by adjusting the voltages applied to the LCVRs to maintain the optimum retardations.

On the other hand, for this arrangement there are two main disadvantages: (1) a LC cannot generate four independent polarization states and (2) the retardation introduced by a LC is dependent on external factors (i.e. temperature). To take this second fact into account, LCVRs were calibrated just before carrying out measurements and switched on for not more than 10 min. During that time, changes in the plot voltage retardation were not found.

The present system allows us to obtain the polarization properties of static transmission samples (i.e. inhomogeneous films [49]) and it can also be applied to the analysis of some *in vitro* biological elements [50]. In reflection mode it could be used in the spatial resolution of substrate media and samples with anisotropic layers [2], in the study of scattering effects in rough surfaces [51] and to obtain important polarization characteristics of *in vitro* samples [52].

Finally, with slight modifications (i.e. changing the detector for a CCD camera in the recording state or introducing a scanning unit), a Mueller-matrix imaging polarimeter [12, 13, 34, 35, 53] can be designed. These kind of systems are oriented to measure the spatial polarization properties of systems by using 16 independent images.

Acknowledgments

This research was supported by Dirección General de Investigación Científica y Técnica (Spain) grants PB94-1138 and PB97-1056. The author thanks Pablo Artal for helpful suggestions and his assistance during the research. The technical assistance of I Miró was very important and discussions with J J Gil were also useful.

References

[1] Chipman R A 1995 Polarimetry *Handbook of Optics* 2nd edn, vol 2, ed M Bass (New York: McGraw-Hill) ch 22
[2] Azzam R M A and Bashara N M 1992 *Ellipsometry and Polarized Light* (New York: North-Holland)
[3] Azzam R M A 1995 Ellipsometry *Handbook of Optics* 2nd edn, vol 2, ed M Bass (New York: McGraw-Hill) ch 27
[4] Bernabeu E and Gil J J 1985 An experimental device for the dynamic determination of Mueller matrices *J. Opt. (Paris)* **16** 139–41
[5] van Blokland G J 1985 Ellipsometry of the human retina in vivo: preservation of polarization *J. Opt. Soc. Am.* A **2** 72–5
[6] Azzam R M A 1978 Photopolarimetric measurement of the Mueller matrix by Fourier analysis of a single detected signal *Opt. Lett.* **2** 148–50
[7] Hauge P S 1978 Mueller matrix ellipsometry with imperfect compensators *J. Opt. Soc. Am.* **68** 1519–28
[8] Hauge P S 1980 Recents developments in instrumentation in ellipsometry *Surf. Sci.* **96** 108–40
[9] Aspnes D E and Studna A A 1975 High precision scanning ellipsometer *Appl. Opt.* **14** 220–8
[10] Thompson R C, Bottinger J R and Fry E S 1980 Measurement of polarized light interactions via the Mueller matrix *Appl. Opt.* **19** 1323–32
[11] Delplancke F 1997 Automated high-speed Mueller matrix scatterometer *Appl. Opt.* **36** 5388–95
[12] Fendrich T, Fischer S K and Bille J F 1994 Development of an electro-optical ellipsometer with aplication in ophthalmology *Proc. SPIE* **2079** 76–82
[13] Pelz B C E, Weschenmoser C, Goelz S, Fischer J P, Burk R O W and Bille J F 1996 *In vivo* measurement of the retinal birefringence with regard on corneal effects using an electro-optical ellipsometer *Proc. SPIE* **2930** 92–101
[14] Wong C F 1979 Birefringence measurement using a photoelastic modulator *Appl. Opt.* **18** 3996–9
[15] Drevillon B, Perrin J, Marbot R, Violet A and Dalby J L 1982 Fast polarization modulated ellipsometer using a microprocessor system for digital Fourier analysis *Rev. Sci. Instrum.* **53** 969–77
[16] Modine F A, Jellison G E Jr and Gruzalski G R 1983 Errors in ellipsometry measurements made with a photoeleastic modulator *J. Opt. Soc. Am.* **73** 892–900
[17] Jellison G E Jr and Modine F A 1997 Two-modulator generalized ellipsometry: experiment and calibration *Appl. Opt.* **36** 8184–9
[18] Jellison G E and Modine F A 1997 Two-modulator generalized ellipsometry: theory *Appl. Opt.* **36** 8190–8
[19] Azzam R M A 1982 Division-of-amplitude photopolarimeter (DOAP) for the simultaneous measurement of all four Stokes parameters of light *Opt. Acta* **29** 685–9
[20] Krishnan S 1992 Calibration, properties and applications of the division-of-amplitude photopolarimeter at 632.8 and 1523 nm *J. Opt. Soc. Am.* A **9** 1615–22
[21] Krishnan S and Nordine P C 1994 Mueller-matrix ellipsometry using the division-of-amplitude photopolarimeter: a study of depolarization effects *Appl. Opt.* **33** 4184–92
[22] Compain E and Drevillon B 1998 High-frecuency modulation of the four states of polarization of light with a single phase modulator *Rev. Sci. Instrum.* **69** 1574–80
[23] Compain E and Drevillon B 1998 Broadband division-of-amplitude polarimeter based on uncoated prisms *Appl. Opt.* **37** 5938–44
[24] Cui Y and Azzam R M A 1996 Sixteen-beam grating-based division-of-amplitude photopolarimeter *Opt. Lett.* **21** 89–91
[25] Saleh B E A and Teich M C 1991 *Fundamentals of Photonics* (New York: Wiley)
[26] Krishnan S and Nordine P C 1996 Fast ellipsometry and Mueller matrix ellipsometry using the division-of-amplitude photopolarimeter *Proc. SPIE* **2873** 152–6
[27] Liu J and Azzam R M A 1997 Polarization properties of corner-cube retroreflectors: theory and experiment *Appl. Opt.* **36** 1553–9
[28] Zhuang Z, Suh S-W and Patel J S 1999 Polarization controller using nematic liquid crystals *Opt. Lett.* **24** 694–6
[29] Ye C 1995 Construction of an optical rotator using quarter-wave plates and an optical retarder *Opt. Eng.* **34** 3031–5
[30] Ye C and Keränen E 1997 Nonmechanical rotation of a linear polarizer preceding a photodetector *J. Opt. Soc. Am.* A **14** 682–5
[31] Wu C and Wu S 1995 Liquid-crystal-based switchable polarizers for sensor protection *Appl. Opt.* **34** 7221–7
[32] Love G D 1997 Wave-front correction and production of Zernike modes with a liquid-crystal spatial light modulator *Appl. Opt.* **36** 1517–24
[33] Vargas-Martín F, Prieto P and Artal P 1998 Correction of the aberrations in the human eye with a liquid-crystal spatial light modulator: limits to performance *J. Opt. Soc. Am.* A **15** 2552–62
[34] Pezzaniti J L and Chipman R A 1995 Mueller matrix imaging polarimetry *Opt. Eng.* **34** 1558–68
[35] Bueno J M and Artal P 1999 Double-pass imaging polarimetry in the human eye *Opt. Lett.* **24** 64–6
[36] Kliger D S, Lewis J W and Randall C E 1990 *Polarized Light in Optics and Spectroscopy* (San Diego, CA: Academic)
[37] Born M and Wolf E 1980 *Principles of Optics* 6th edn (New York: Pergamon)
[38] Theocaris P S and Gdoutos E E 1979 *Matrix Theory of Photoelasticity (Springer Series in Optical Sciences 11)* (Berlin: Springer)
[39] Shurcliff W A 1962 *Polarized Light: Production and Use* (Cambridge, MA: Harvard University Press)
[40] Morgan F M, Chipman R A and Torr D G 1990 An ultraviolet polarimeter for characterization of an imaging spectrometer polarimetry: radar, infrared, visible, ultraviolet and x-ray *Proc. SPIE* **1317** 384–94
[41] Pezzaniti J L and Chipman R A 1990 Imaging polarimeters for optical metrology polarimetry: radar, infrared, visible, ultraviolet and x-ray *Proc. SPIE* **1317** 280–94
[42] Ambirajan A and Look D C 1995 Optimum angles for a polarimeter: part 1 *Opt. Eng.* **34** 1651–5
[43] Gil J J and Bernabeu E 1987 Obtainment of the polarizing and retardation parameters of a non-depolarizing optical system from the polar decomposition of its Mueller matrix *Optik* **76** 67–71
[44] Gil J J and Bernabeu E 1986 Depolarization and polarization indices of an optical system *Opt. Acta* **33** 185–9
[45] Chipman R A 1989 Polarization analysis of optical systems *Opt. Eng.* **28** 90–9
[46] Jaroñski J W and Kasprzak H T 1999 Generalized algorithm for photoelastic measurements based on phase-steping imaging polarimetry *Appl. Opt.* **38** 7018–25
[47] Bueno J M 1999 Elliptical polariscope for the analysis of highly birefringent samples *Óptica Pura y Aplicada* **1** at press

[48] Bueno J M and Artal P 1999 Polarization and double-pass estimates of the retinal image quality in the human eye *EOS Topical Meetings Digest Series 23* pp 42–3
[49] Rotter L D and Kaiser D L 1995 Polarimetry of inhomogeneous films of anisotropic crystallites: birrefringence in $BaTiO_3$ thin films *J. Opt. Soc. Am.* A **12** 999–1009
[50] Jaroñski J W and Kasprzak H T 1998 Measurements of the corneal birefringence by use of the phase shifting imaging polarimetry *Proc. SPIE* **3579** 133–7
[51] Nee S-M 1996 Polarization of specular reflection and near-specular scattering by a rough surface *Appl. Opt.* **35** 3570–82
[52] Dreher A W, Reiter K and Weinred R N 1992 Spatially resolved birefringence of the retinal never fibre layer assessed with a retinal laser ellipsometer *Appl. Opt.* **31** 3730–5
[53] Gerligang P Y, Le Jeune B, Cariou J and Lotrian J 1995 Spatial homogeneities evaluation of ferrofluid thin plates polarimetric characteristics for active imagery *Opt. Eng.* **34** 1581–8